CHEMISTRY
A EUROPEAN JOURNAL

ChemPubSoc
Europe

DOI: 10.1002/chem.201203887

Borylated Arylisoquinolines: Photophysical Properties and Switching Behavior of Promising Tunable Fluorophores

Vânia F. Pais,[a] Hamdy S. El-Sheshtawy,[b] Rosario Fernández,[c] José M. Lassaletta,[d] Abel Ros,*[d] and Uwe Pischel*[a]

Abstract: A series of nine borylated arylisoquinolines has been prepared with systematic variation in their electronic properties and their photophysical properties were investigated. The color of their fluorescence can be finely tuned by changing the properties of the aryl moiety, which is involved in internal-charge-transfer processes. For example, methoxy-substituted compound **5** showed an intense green emission, whereas dimethylamino-substituted compound **6** showed an orange-red emission. These new fluorophores were tested for their potential as molecular switches with external ionic stimuli, such as protons and fluoride ions. On the one hand, protonation of the isoquinoline moiety led to fluorescence enhancement for compounds that showed weak charge transfer and fluorescence quenching for compounds that showed strong charge transfer. On the other hand, the formation of *ate* complexes with fluoride led to strong fluorescence quenching in all of the investigated cases.

Keywords: boron · fluorescence · fluorides · molecular switches · sensors

Introduction

Fluorophores that contain trisubstituted boron species, such as triarylboranes or aryl boronic acids and their derivatives, have been intensively exploited for applications as luminescent polymeric materials,[1–6] in nonlinear optics,[7,8] as model chromophores for the study of electron transfer,[9,10] and as chemosensors.[11–14] The electron-deficient nature of a trisubstituted boron atom in chromophoric architectures provides possibilities for the coordination of donor ligands through interactions with its vacant p_π orbital. This coordination enables the tuning of the photophysical properties of the system upon the addition of donor ligands, such as fluoride (F^-) ions, thus resulting in chromogenic or fluorescent sensors.[11–13,15] The most widely employed systems are based on internal-charge-transfer processes in the excited state that involve the electron-deficient boron atom, which, upon the coordination of F^-, loses its electron-accepting properties. This process is often accompanied by an "on-off" fluorescence switching.[16,17] Indeed, systems in which "off-on" fluorescence switching[18–20] or a ratiometric emission response[7,21–28] are observed are of great interest for sensing purposes. Other designs have used the classical photoinduced electron-transfer approach,[29–31] by integrating electron-donating fluorophores with electron-accepting triarylboranes.[32] An additional functional aspect of fluorescent organoborane compounds is the implementation of switches with multiple emissive states.[33] Notably, another abundantly employed design principle for fluorescent fluoride chemosensors relies on anionic interactions with activated NH moieties (urea, thiourea, aminonaphthalimides, etc.).[34–44]

Herein, we exploited a new class of fluorophores with boronic ester groups that were structurally and electronically integrated with arylisoquinolines. These compounds were prepared by using a recently developed borylation method of broad synthetic scope.[45] The resulting fluorophores showed electronically tunable internal-charge-transfer (ICT) fluorescence emission in an ample spectroscopic window and could be switched by protonation of the isoquinoline or the formation of fluoroboronate complexes with the boronic acid ester.

[a] V. F. Pais, Prof. Dr. U. Pischel
Centro de Investigación en Química Sostenible (CIQSO) and
Departamento de Ingeniería Química
Química Física y Química Orgánica
Universidad de Huelva, Campus de El Carmen s/n
21071 Huelva (Spain)
Fax: (+34) 959-21-99-83
E-mail: uwe.pischel@diq.uhu.es

[b] Dr. H. S. El-Sheshtawy
Chemistry Department, Faculty of Science
South Valley University, 83523 Qena (Egypt)

[c] Prof. Dr. R. Fernández
Departamento de Química Orgánica, Universidad de Sevilla
C/Prof. García González 1, 41012 Sevilla (Spain)

[d] Prof. Dr. J. M. Lassaletta, Dr. A. Ros
Instituto de Investigaciones Químicas (CSIC-US)
C/Américo Vespucio 49, 41092 Sevilla (Spain)
Fax: (+34) 954-46-05-65
E-mail: abel.ros@iiq.csic.es

Supporting information for this article is available on the WWW under http://dx.doi.org/10.1002/chem.201203887.

Results and Discussion

Molecular design: A series of borylated arylisoquinolines (**1**–**9**, Scheme 1), the fluorescence of which can be addressed in two ways, that is, by the addition of protons (H^+) or

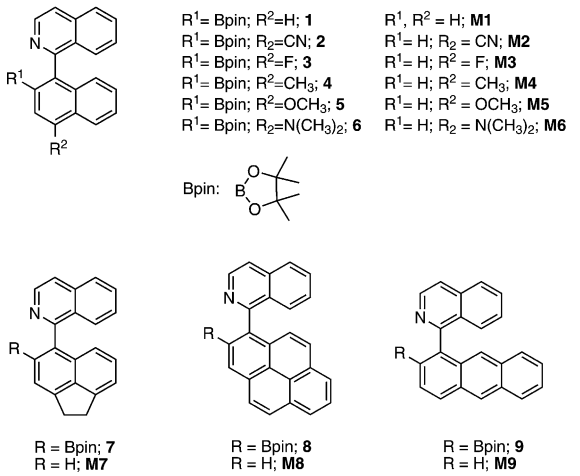

Scheme 1. Structures of borylated arylisoquinolines **1**–**9** and their respective models (**M1**–**M9**).

anions (F^-),[36,46,47] was explored. The design principle (Scheme 2) rested on three pillars: 1) The coordination of F^- ions to the boron center, thus giving rise to tetracoordinated fluoroboronate substituents with strong electron-donating character; 2) the protonation of the isoquinoline moiety, thereby increasing its electron-demanding character; and 3) the possibility of observing fluorescence based on internal charge transfer (ICT).

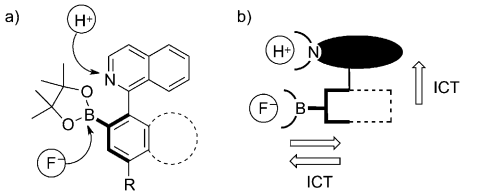

Scheme 2. Molecular design of dually switchable borylated arylisoquinolines: a) general structure and indication of the input recognition sites and b) schematic representation of possible ICT interactions.

For the purpose of studying the electronic effects on the ICT properties of these compounds, a set of compounds with various aryl moieties (naphthyl, acenaphthyl, pyrenyl, anthryl) and, in the case of the naphthyl moieties, substitution with electron-withdrawing or electron-donating groups, were prepared. The chosen synthetic approach (see below) yielded the borylated target compounds, as well as their corresponding boron-free arylisoquinolines (**M1**–**M9**), which served as photophysical models.

Synthesis of borylated arylisoquinolines: The boron center was integrated as a boronic acid pinacol ester. Recently, we reported a convenient synthetic access to *ortho*-borylated arylisoquinolines through an iridium(III)-catalyzed nitrogen-directed reaction,[45] thereby obtaining the herein-exploited compounds **1**, **4**, **7**, and **8** in excellent yields. The scope of this recently introduced method was further extended herein, thereby yielding borylated arylisoquinolines with electron-withdrawing (**2** and **3**) and electron-donating substituents (**5** and **6**) at the 4 position of the naphthalene moiety, as well as the borylated 1-(anthracen-1-yl)isoquinoline (**9**). These reactions worked well at 55 °C, thus affording the desired *ortho*-borylation products in good-to-excellent yields (Scheme 3). The borylation of cyano derivative **M2** required elevated reaction temperatures (80 °C) to afford the desired product (**2**). This result was attributed to the ability of the cyano group to compete with the N(sp^2) atom of the isoquinoline moiety for the vacant coordination site of the catalyst.[48]

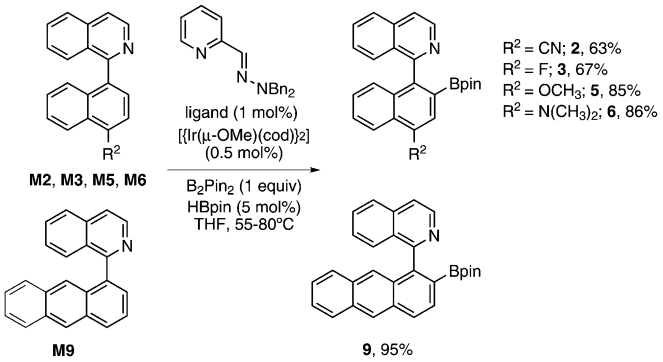

Scheme 3. Directed *ortho*-borylations of models **M2**, **M3**, **M5**, **M6**, and **M9**.

The *ortho*-borylation step was performed with the corresponding arylisoquinolines. Hence, the model compounds (**M1**–**M9**) were precursors of the final borylated products and, thus, were directly available from this synthetic sequence. The synthesis of precursors **M1**, **M4**, **M7**, and **M8** has been reported elsewhere.[45] The newly prepared arylisoquinolines (**M2**, **M3**, **M5**, **M6**, and **M9**) were obtained from their corresponding haloarenes by palladium-catalyzed one-pot borylation/Suzuki-coupling, following Buchwald's method (Scheme 4).[49]

Structural characterization: The ^1H and ^{11}B NMR data for compounds **1**–**9** (see the Supporting Information) provided evidence for the absence of intramolecular B–N interactions, most likely for steric reasons:[45] The ^{11}B NMR signal appeared within the range $\delta = 30$–31 ppm for all of these compounds, typical for tricoordinated sp^2 boron atoms.[50] On the contrary, for a B–N interaction, which would imply sp^3 hybridization of the boron atom, strong shielding and an upfield shift to $\delta = 13$–15 ppm should have been detected.[50] Another indicator of the absence of B–N interactions was

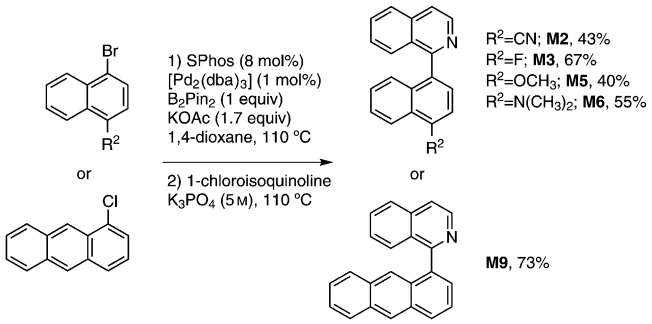

Scheme 4. Synthesis of precursors **M2**, **M3**, **M5**, **M6**, and **M9**.

the ^{1}H signal of the pinacolate methyl groups. These protons appeared, without exception, in the region $\delta = 0.74$–1.01 ppm. The formation of an internal Lewis adduct should have led to deshielding ($\delta \approx 1.40$–1.45 ppm),[45] which was not observed. Further compelling evidence for the absence of B–N interactions in the case of compound **1** came from a recently reported crystal structure.[45]

UV/Vis absorption and fluorescence properties: The most important photophysical properties of compounds **1**–**9** in MeCN are summarized in Table 1. Representative absorption and fluorescence spectra are shown in Figure 1 (all other spectra can be found in the Supporting Information). The UV/Vis absorption spectra showed major bands in the region 250–400 nm. In the case of compounds **8** and **9**, their spectra were complemented by the typical signatures of pyrene and anthracene at around 340 and 370 nm, respectively (see the Supporting Information). The fluorescence spectra were generally dominated by broad and red-shifted long-wavelength (LW) emission bands. Moreover, in general, a weak and blue-shifted short-wavelength (SW) emission was also notable, except for compound **2**, which showed only one emission band. Figure 2 shows a photograph of the emission colors of compounds **1**–**9**. Whereas the emissions of compounds **1**–**3** were hardly visible, compounds **4**–**9** showed appreciable brightness, which was especially evident for compounds **5**, **6**, and **8**.

Table 1. UV/Vis absorption and fluorescence properties of compounds **1**–**9** in MeCN.

	λ_{abs} [nm]	ε [$M^{-1}cm^{-1}$][a]	λ_{fl} [nm]	Φ_f[b]	$I_{fl}(LW)/I_{fl}(SW)$	τ_{fl} [ns] (%)[c]
1	284	9500	368, 492	0.01	3	0.32 (98.3)
2	309	10200	437	0.01	–[d]	0.26 (98.1)
3	286	8250	362, 494	0.02	21	1.00 (91.8)
4	287	9700	386, 502	0.04	25	2.51 (98.5)
5	309	9100	424, 532	0.43	123	7.81 (81.2)
6	323	6200	420, 608	0.36	149	6.11 (100)
7	291	8300	417, 527	0.20	41	7.95 (100)
8	341	33000	391, 412, 528	0.27	29	3.32 (100)
9	371	4800	428, 571	0.10	6	3.28 (100)

[a] Value refers to λ_{abs}. [b] Fluorescence quantum yield. [c] Fluorescence lifetime of the main component (weight is given in parentheses). [d] Only one fluorescence band was observed.

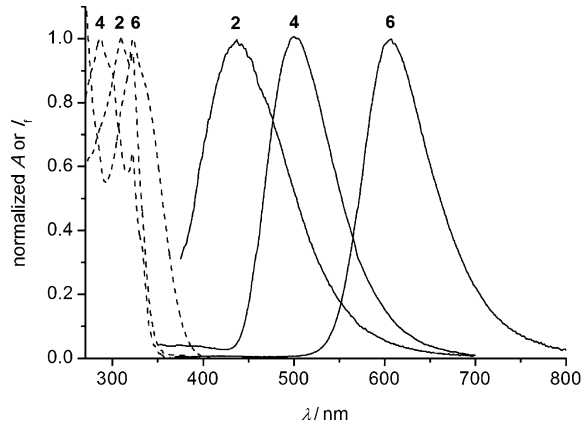

Figure 1. Normalized UV/Vis absorption spectra (dashed lines) and fluorescence spectra (solid lines) of compounds **2**, **4**, and **6** in MeCN.

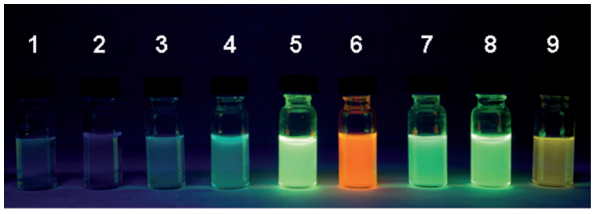

Figure 2. Fluorescence colors of solutions (about 3.2 mM) of compounds **1**–**9** in MeCN. The brightness of the emission depends on the product $\Phi_f \times \varepsilon(\lambda_{abs})$.

To gain more insight into the nature of the red-shifted LW emission, it appeared reasonable to have a closer look at its spectral position in relation to the aryl oxidation potential. Figure 3 shows a plot of the half-wave oxidation potential of the aryl residues[51,52] (see Table 2) versus the energies that correspond to the LW maximum. A clear trend is evident (linear regression; $r = 0.963$, $n = 9$): The easier the

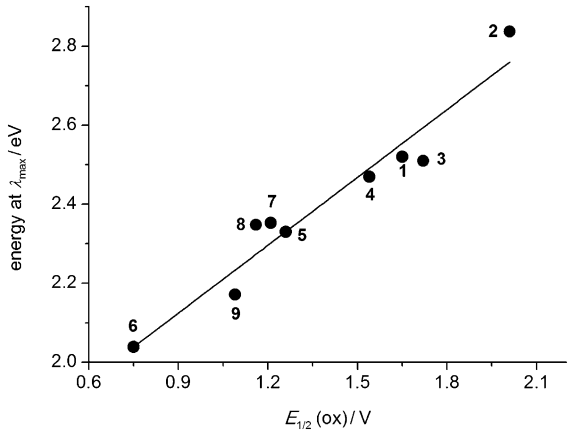

Figure 3. Linear plot of the energy that corresponds to the principal fluorescence emission maximum versus the half-wave oxidation potential of the aryl moiety.

Table 2. Redox potentials, solvatochromic effects, and fluoride-binding constants for compounds **1**–**9**, as well as their fluorescence modulation upon the addition of TFA or Bu_4NF, in MeCN.

	E_{ox} [V][a]	$\Delta\lambda$ [nm][b]	K [M^{-1}][c]	Q [%][d] (TFA)	Q [%][d] (Bu_4NF)
1	1.65[e]	1	$(6.9\pm0.6)\times10^3$	–[f]	70
2	2.01[e]	−2	$>10^6$[g]	–[f]	93
3	1.72[e]	3	$(6.9\pm0.9)\times10^4$	5	85
4	1.54[e]	5	$(3.7\pm0.1)\times10^3$	59	89
5	1.26[e]	11	$(2.1\pm0.1)\times10^4$	96	96
6	0.75[h]	26	$(9.5\pm0.3)\times10^3$	99	96
7	1.21[e]	15	$(3.3\pm0.6)\times10^3$	87	78
8	1.16[h]	19	$(1.9\pm0.1)\times10^4$	91	86
9	1.09[h]	27	$(1.4\pm0.2)\times10^4$	96	98

[a] Half-wave oxidation potential of the aryl model (versus SCE in MeCN): **1**=naphthalene, **2**=1-cyanonaphthalene, **3**=1-fluoronaphthalene, **4**=1-methylnaphthalene, **5**=1-methoxynaphthalene, **6**=1-(*N*,*N*-dimethylamino)naphthalene, **7**=acenaphthene, **8**=pyrene, **9**=anthracene. [b] Solvatochromic shift of the LW fluorescence maximum upon switching from toluene to MeCN. [c] 1:1 Binding constant of fluoride that resulted in the formation of a fluoroboronate complex, as measured by fluorescence titration. [d] Fluorescence quenching of the LW emission band (measured at the maximum wavelength) upon the addition of 10 equivalents of TFA or 60 equivalents of Bu_4NF. [e] See ref. [52]. [f] Fluorescence enhancement was observed by a factor of 3.6 and 4.3 for compounds **1** and **2**, respectively. [g] Lower limit, too large to be measured accurately. [h] See ref. [51].

aryl group is to oxidize, the lower the energy level of the fluorescent state. For example, compound **6**, which contained a 4-(*N*,*N*-dimethylamino)naphthyl moiety ($E_{1/2}(ox)=0.75$ V versus SCE in MeCN),[51] showed the most red-shifted emission, with $\lambda_{max}=608$ nm. On the other hand, compound **2**, which contained a hard-to-oxidize 4-cyanonaphthyl residue ($E_{1/2}(ox)=2.01$ V versus SCE in MeCN),[52] had its only emission band at 437 nm. Based on this trend, we inferred that ICT, through the participation of the aryl residue, was a decisive factor in determining the photophysical behavior of these compounds. The often-observed dual fluorescence signature of biaryl fluorophores has been interpreted along similar lines, by invoking an equilibrium between the locally excited (LE) and ICT states.[53] The geometry of these latter states, which are often discussed as "twisted" versus "planar" ICT states, has been the subject of some controversy in the literature.[53,54] As can be clearly seen from the $I_{fl}(LW)/I_{fl}(SW)$ ratio, the ICT state is dominant in MeCN for the compounds investigated herein.

The occurrence of ICT phenomena in the excited state was further supported by the observation of significant solvatochromic effects on the spectroscopic position of the LW emission maximum (Table 2, Figure 4, and the Supporting Information).[55] In accordance with these results, the compounds with the most pronounced ICT (**6**, **8**, and **9**) showed the largest bathochromic shifts of the LW emission band upon switching from non-polar toluene to polar MeCN: $\Delta\lambda=19$–27 nm. For the other compounds (**1**–**5** and **7**), the effects were significantly smaller or even negligible ($\Delta\lambda=-2$ to 15 nm). For representative compounds with negligible ICT (**2**), moderate ICT (**4**), and pronounced ICT (**6** and **9**), a more detailed analysis of the solvent effect on the position

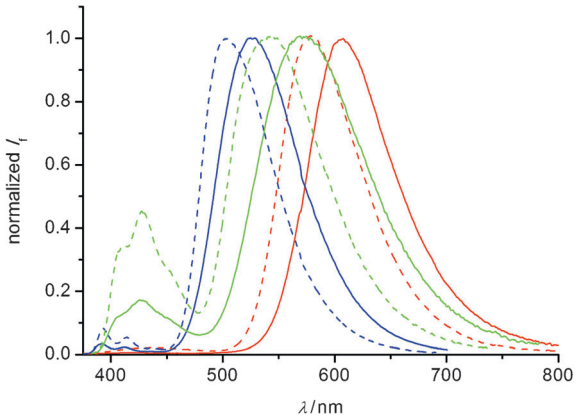

Figure 4. Solvent effects on the fluorescence spectra of compounds **6** (red), **8** (blue), and **9** (green). Dashed lines correspond to the spectra in toluene and the solid lines to the spectra in MeCN; all spectra are normalized to 1 at their maximum intensity.

of the LW emission band was performed. Figure 5 shows a plot of the LW emission maximum (in cm^{-1}) versus the Dimroth–Reichardt $E_T(30)$ parameter[56] for selected compounds

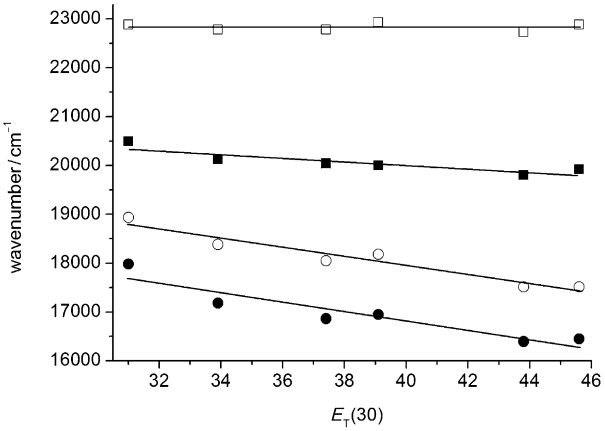

Figure 5. Linear plot of the LW emission maximum versus the $E_T(30)$ solvent parameter of compounds **2** (□), **4** (■), **6** (●), and **9** (○).

in *n*-hexane, toluene, $CHCl_3$, THF, MeCN, and DMF. A linear correlation ($r=0.856$–0.958) was observed for compounds **4**, **6**, and **9**: The higher the $E_T(30)$, the lower the emission energy. The gradient of the slope of the plots should give some semi-quantitative insight in the degree of ICT, which is supportive of the conclusions shown above. Thus, for compound **4**, a 2.5-times shallower slope than for compounds **6** and **9**, with pronounced ICT character, was obtained. However, in line with the negligible ICT character of compound **2**, no influence of the solvent was observed. Using the Lippert–Mataga parameter (Δf)[57,58] for the analysis led to similar plots (see the Supporting Information), albeit with poorer linear-regression parameters.

Interestingly, the SW band (where visible) showed no significant solvatochromic effect, as clearly observed for com-

pound **9** (Figure 4). Hence, the SW bands were assigned to a locally excited (LE) state. Furthermore, the relative intensity of the SW band increased with decreasing solvent polarity (e.g., for compound **9**, $I_{fl}(LW)/I_{fl}(SW) \approx 6$ versus 2 in MeCN and toluene, respectively). This result was in line with the assignment of an ICT state to the LW band, because a lower solvent polarity would destabilize the ICT state and, thus, emission from the LE state gained more weight.

In the overall series, the fluorescence quantum yield (Φ_f; Table 1) was the highest for compound **5** ($\Phi_f = 0.43$). For the naphthalene derivatives with more-positive aryl oxidation potentials (**1**–**4**), much-lower emission quantum yields were noted ($\Phi_f < 0.05$). This result provides further indication of the importance of ICT phenomena, especially for compounds with easily oxidizable aryl groups. Compound **6**, which had the energetically lowest-lying emissive ICT state, showed a small drop in quantum yield ($\Phi_f = 0.36$) compared to compound **5**. This behavior can be understood by the energy-gap law: The lower lying the emissive state, the more competitive the non-radiative deactivation processes. Similar trends for the emission quantum yields were noted for derivatives with aryl residues with different extents of conjugation (**1**, **7**, **8**, and **9**). Anthracene derivative **9** (with the lowest-lying ICT state in this set) showed a significantly lower emission quantum yield compared to acenaphthene derivative **7** or pyrenyl-substituted derivative **8** (Table 1).

The lifetimes of the ICT emission were measured as complementary data and they followed a similar trend to the quantum yields (Table 1; for detailed analysis, see the Supporting Information). The emission of the compounds with the weakest ICT was very short lived ($\tau < 0.4$ ns for compounds **1** and **2**) and it reached a maximum for compounds with significant ICT character ($\tau \approx 8$ ns for compounds **5** and **7**) with some decrease for compounds with energetically low-lying ICT states (**6**: $\tau \approx 6$ ns; **8** and **9**: $\tau \approx 3$ ns).

Density functional theory (DFT) calculations of compounds 1–6: The direct participation of the aryl residue in the observed fluorescence behavior was further corroborated by the results of DFT calculations. For consistency and to facilitate the direct comparison of these results, calculations were performed on the naphthalene-derived subseries of compounds **1**–**6**. Contour plots of the frontier orbitals of the optimized structures (at the B3LYP/6-31+G(d,p) level of theory) of three selected examples (which were differentiated by the electron-donating propensity of their naphthyl residue) are shown in Figure 6. For compounds **4** and **6**, the HOMO was localized over the borylated aryl residue, whereas the isoquinolinyl group made the largest contribution to the LUMO. The same picture was obtained for compounds **1**, **3**, and **5** (see the Supporting Information), which strongly suggested that the ICT involved an aryl moiety as a donor and the isoquinolinyl group as an acceptor. Compound **2** was an exception, in which both the HOMO and LUMO were mainly located on the borylated aryl residue, in agreement with the assignment of a LE state as the lowest-energy transition.

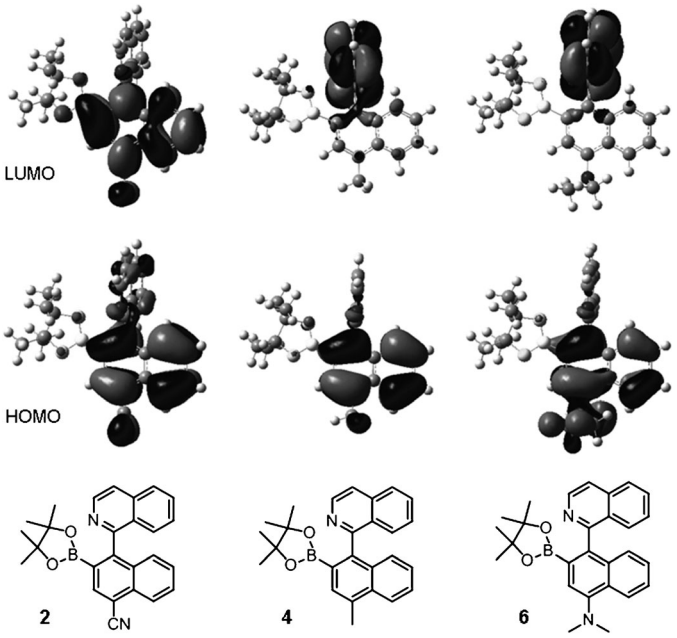

Figure 6. HOMO and LUMO contour plots of the optimized molecular geometries (at the B3LYP/6-31+G(d,p) level of theory) of compounds **2**, **4**, and **6**.

The energies of the frontier orbitals in this series corresponded very well with the expected values, based on the substituent effects (Figure 7). For example, cyano-substituted compound **2** had the lowest-lying HOMO because it was the hardest to oxidize. On the other hand, the *N*,*N*-dimethylamino substituent, as the strongest electron-donating group, gave rise to the highest-lying HOMO (easiest to oxidize) for compound **6**. Moreover, the trends in the LUMO energies of the compounds in the naphthalene subseries (**1**–**6**) also corresponded to their expected electronic properties. Compound **2**, as the easiest reducible compound, had the lowest-lying LUMO (Figure 7), with the highest contribution from the Bpin–cyanonaphthalene residue. The major contribution in the other compounds (**1** and **3**–**6**) came from the isoquinoline moiety and, thus, they showed comparable and consistently higher LUMO energies. This very satisfactory correlation between the electronic structure and the calculated

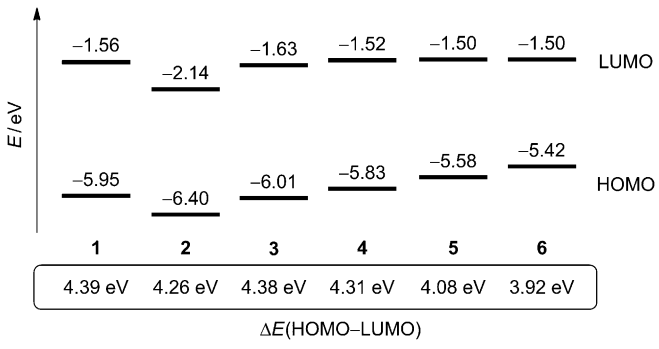

Figure 7. DFT-calculated HOMO and LUMO energies of naphthalene-derived compounds **1**–**6**.

energies gave us confidence for also comparing their HOMO–LUMO energy differences (ΔE). Thus, we found that the relative trend in the energetic position of the LW emission band was correctly expressed in qualitative terms by the calculations (Figure 7). Again, compound **2** was the only exception, which could be reasoned by the different localization of the LUMO (Figure 6).

Comparison with non-borylated analogues: For the sake of comparison and for confirming the role of the boronic ester substituent, non-borylated models **M1**–**M9** were also included in this study. Their photophysical data in MeCN are summarized in Table 3. The absorption spectra did not change dramatically in the absence of the Bpin substituent (see the Supporting Information). However, obviously, the fluorescence spectra only showed one (generally weak) emission band, close to the SW band of the corresponding borylated derivative (where observable). This result is shown in Figure 8 for methyl-substituted naphthalene derivative **M4** as an example. Compound **M6** was an exception, which showed a band that was spectroscopically unrelated with the observed very weak SW emission for compound **6** (Table 3 and Supporting Information). In general, the emission quantum yields were much lower than those observed for the borylated analogues, often lower than 0.01. The same trend also applied to the emission lifetimes, except for compounds with weak ICT character in their borylated derivatives. From these observations, we concluded that boron substitution indeed played an important role in establishing the emissive properties of the borylated arylisoquinolines. However, upon protonation (the addition of 10 equivalents of trifluoroacetic acid, TFA), the isoquinoline moiety turned into a cationic isoquinolinium group, a much stronger electron acceptor, and, again, broad red-shifted LW emission bands became visible at similar positions as observed for the borylated analogues (Figure 8 for **M4**H$^+$ as an example). This behavior was assigned as the formation of an ICT state, which was also supported by the appearance of new red-shifted absorption features for the protonated model compounds at $\lambda = 330$–450 nm (see the Supporting Information). Compound **M6** was an exception, which only showed fluorescence quenching of the band at $\lambda = 553$ nm upon protonation. The new emissive ICT state was presumably so low-lying that its quantum yield was very small because of a strongly competing non-radiative decay process (energy-gap law). A similar reasoning also applied to anthryl derivative **M9**, for which a very small new emission at $\lambda = 632$ nm was observed upon protonation.

Table 3. UV/Vis absorption and fluorescence properties of arylisoquinolines **M1**–**M9** in MeCN.

Model	λ_{abs} [nm]	ε [M^{-1}cm^{-1}][a]	λ_{fl} [nm]	λ_{fl} [nm][b]	Φ_f[c]	τ_f [ns][d]
M1	282	10200	370	501	0.01	4.96
M2	312	9800	431	465	<0.01	1.93
M3	285	10150	376	493	<0.01	3.75
M4	287	10800	388	515	<0.01	1.70
M5	310	9800	425	580	<0.01	0.64
M6	323	6600	553	–[e]	0.06	3.92
M7	297	9700	418	560	<0.01	0.53
M8	341	33100	439	599	0.02	0.89
M9	362	7700	433	632[f]	0.09	1.00

[a] Value refers to λ_{abs}. [b] Fluorescence maximum of the red-shifted LW band on the addition of 10 equivalents of TFA. [c] Fluorescence quantum yield of the unprotonated compound. [d] Multiexponential decays (see the Supporting Information); lifetimes are stated as average fluorescence lifetimes. [e] Only quenching was observed, with no new LW bands. [f] Maximum of a very weak new fluorescence band.

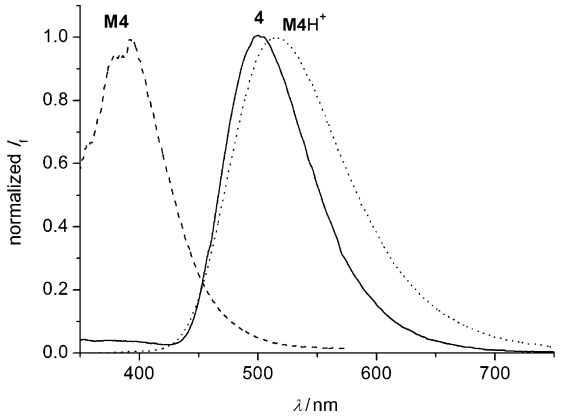

Figure 8. Comparison of the normalized fluorescence spectra of compounds **M4**, **M4**H$^+$ (with 10 equivalents of TFA), and **4** in MeCN.

Fluorescence modulation by the addition of an acid: Based on the photophysical effects upon protonation of the non-borylated model compounds (see above), it was of interest to examine the fluorescence response of borylated analogues **1**–**9** on the addition of acid (10 equiv TFA). Their response was clearly dependent on the electronic conditions of the system. Compounds **1**–**3**, which contained aryl residues that were either weak electron donors/acceptors (**1**, **3**) or strong acceptors (**2**), yielded strong-to-moderate fluorescence enhancements (for compound **1**, see Figure 9 and Table 2) or only showed very minor quenching effects (compound **3**). All of the other borylated derivatives (**4**–**9**) gave moderate-to-almost-quantitative fluorescence quenching of the LW band, that is 59% quenching for compound **4** and 87–99% quenching for compounds **5**–**9** (for compound **6**, see Figure 9, Table 2, and the Supporting Information).

These observations were interpreted as follows: Derivatives **1** and **2** only showed minor inherent excited-state ICT character, owing to the protonation of the isoquinoline group, which transformed this moiety into a strongly electron-accepting isoquinolinium cation. The result was an increased degree of ICT, which was accompanied by fluorescence enhancement. In agreement with a slightly narrowed energy gap, red-shifts of the emission band of compound **1** by about 7 nm and of compound **2** by about 20 nm were noted.

In principle, one could anticipate this behavior for the complete series of compounds **1**–**9**. However, for the derivatives in which a pronounced ICT was already noted for the

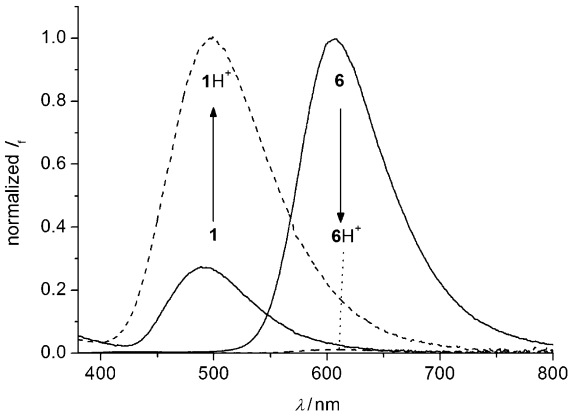

Figure 9. Effect of the addition of 10 equivalents of TFA to solutions of compounds **1** and **6** in MeCN. The spectra were normalized to 1 at their maximum intensity. The solid lines correspond to the spectra of the unprotonated compounds and the dashed lines correspond to the spectra of the protonated compounds.

unprotonated compounds (especially for compounds **5**–**9**), the additional energetic stabilization of the ICT state by isoquinolinium formation favored their preferential deactivation through non-radiative processes (energy-gap law). Hence, the emission quantum yield of the new ICT state (upon protonation of the isoquinoline) was drastically decreased, thus resulting in the observed fluorescence quenching. The observation of fluorescence enhancement or quenching in the investigated series is a fine balance between the energetic positioning of the ICT states of the protonated compounds.[59]

The fluorescence response to a large excess of selected metal cations (60 equiv Na^+, Ag^+, Mg^{2+}, Pb^{2+}, and Zn^{2+}) was also investigated for some representative compounds (**2**, **4**, **6**, and **9**; for detailed data, see the Supporting Information). With Na^+ ions, no fluorescence modulation was observed. However, divalent metal cations (such as Pb^{2+} or Zn^{2+}) led, in some cases (compounds **6** and **9**), to very strong fluorescence quenching (81–100%). Such effects are often interpreted as being the result of heavy-atom-induced intersystem crossing (Pb^{2+}) or redox quenching (d-metal cations, like Zn^{2+}). However, because many of these cations form Brønsted acidic aquo complexes with trace water or hydrate water, the observed fluorescence quenching may actually be the result of isoquinoline protonation. The observed fluorescence enhancement of compound **2** (by up to 400%) on the addition of Pb^{2+} or Zn^{2+} is analogous to the observations made on the addition of TFA and contrary to the expected nature of the quenching by these metal cations. Hence, these combined observations provide strong indication that protonation is indeed the decisive factor in the fluorescence modulation. Thus, the effects of the metal ions themselves are postulated to be of minor importance.

The fluorescence experiments in this study were performed in MeCN as the solvent. To show that the fluorescence response upon protonation should also be observable in aqueous media, the experiments were repeated for compounds **6** and **9** in a 1:1 mixture of MeCN/water. As expected, upon the addition of 10 equivalents of TFA, strong fluorescence quenching (about 90%) was observed.

Fluoride-ion-binding properties and photophysical effects: The use of boron-substituted fluorophores in chemosensing is often connected to their interactions with fluoride ions (F^-) in a Lewis acid/Lewis base reaction. The binding constants for the formation of 1:1 adducts upon the addition of tetra-*n*-butylammonium fluoride are listed in Table 2 (for an example titration curve of compound **9**, see Figure 10). For

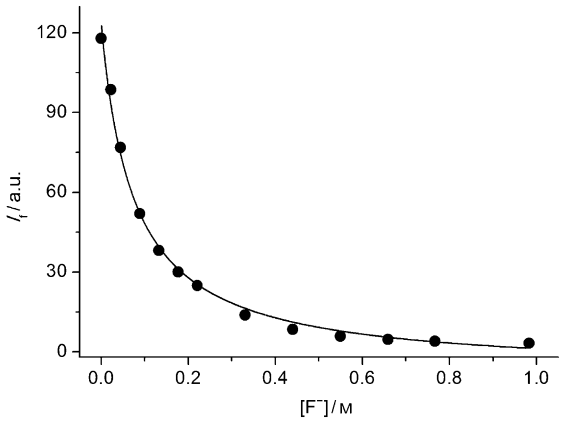

Figure 10. Fluorescence titration curve of compound **9** in MeCN with Bu_4NF. The intensity of the LW emission band was monitored. The solid line corresponds to the fitting according to 1:1 binding.

most compounds, the values varied between 3×10^3 and $2\times10^4\,M^{-1}$. However, derivatives **2** and **3** showed larger binding constants, exceeding $10^6\,M^{-1}$ in the case of cyano-substituted derivative (**2**). This result was attributed to the electron-withdrawing mesomeric effect of the CN substituent and the electron-withdrawing inductive effect of the F substituent, both of which increased the Lewis acidity of the boron atom. Similar trends have been reported for other boronic acid derivatives.[60,61] Globally, the observed binding affinities for fluoride are comparable with that of other boronic acid derivatives in organic solvents.[13] For example, for compound **9**, the notion of the formation of a stable 1:1 adduct with F^- was further supported by its unambiguous detection by electrospray ionization mass spectrometry, which showed a corresponding peak at $m/z=450$ (see the Supporting Information). Similar verifications by mass spectrometry were made for a F^- adduct of ferrocenyl boronic acid ester.[62] The formation of the **9**·F^- adduct was also followed by ^{11}B NMR spectroscopy. The addition of 0.5 equivalents of Bu_4NF to a solution of compound **9** resulted in the immediate appearance of a ^{11}B signal at about $\delta=7.0$ ppm (Figure 11). When 1.0 equivalent of Bu_4NF was added, almost all of the signal at $\delta=31.1$ ppm, which corresponded to tricoordinated boron in the boronic acid ester, had disappeared and only the resonance signal at $\delta=7.0$ ppm, which was assigned to the tetracoordinated boron in the fluorobor-

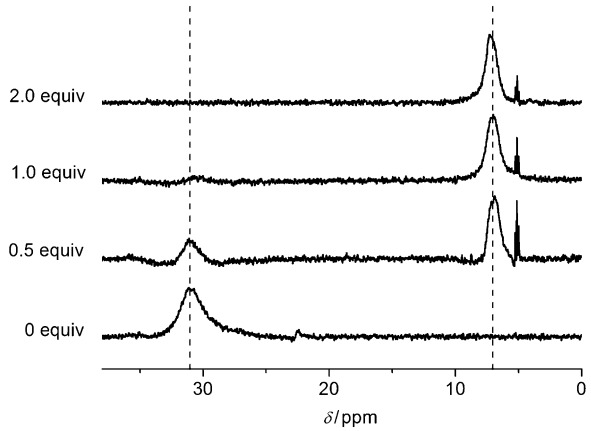

Figure 11. ^{11}B NMR spectra of compound **9** in [D_3]MeCN upon the successive addition of Bu_4NF (0.5–2.0 equiv). The spectra were recorded in boron-free NMR tubes.

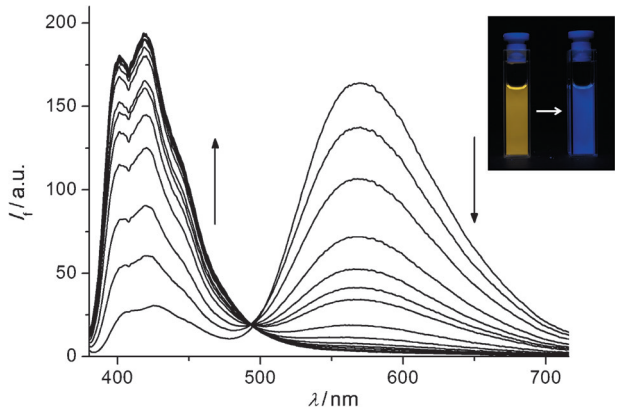

Figure 12. Fluorescence titration of compound **9** in MeCN with Bu_4NF. The LW band at $\lambda_{max}=571$ nm diminished and a new SW band at $\lambda_{max}=420$ nm developed. At $\lambda=494$ nm, an isoemissive point was maintained throughout the titration. Inset shows the change in emission color upon the addition of fluoride.

onate complex, was observable. In a recent report, similar *ate* complexes showed ^{11}B NMR signals in the range $\delta=7$–8 ppm.[63] The observed upfield shift reflected the change in the coordination number, as well as the geometry at the boron center.

The binding event was accompanied by strong-to-almost-quantitative fluorescence quenching (Table 2). The formation of the F^- adduct turned the boronic acid ester into an electron-donating fluoroboronate substituent. The related fluorodihydroxyboronate substituent ($B(OH)_2F^-$) is one of the strongest known inductively donating groups.[13] Hence, it can be assumed that the F^- coordination results in increased electron-donating propensity of the aromatic moieties, which leads to an energetically lower-lying ICT state and, hence, to fluorescence quenching, according to the energy-gap law. Alternatively, excited-state electron transfer from the fluoroboronate–aryl residue to the isoquinoline part could be responsible for the quenching mechanism.[14] Electron- or charge-transfer-induced fluorescence quenching upon the formation of a fluoroboronate has precedence in the literature.[64] By taking a closer look at compound **2**, it was obvious that the LUMO did not involve the isoquinoline group (as for the other naphthalene-derived compounds), but instead involved the vacant boron p_π orbital. As is often observed for triarylboranes, F^- binding quenched the transition that involved the LUMO.[21,23]

Interestingly, compound **9** showed exceptional response that was well-differentiated from the generally observed on-off fluorescence modulation (Figure 12). The quenching of the LW emission band at 571 nm was accompanied by the growth of a blue-shifted SW band at about 420 nm, thus giving access to ratiometric sensing. Similar observations have occasionally been discussed for other boron-containing fluorophores.[7,21–28] DFT calculations (see the Supporting Information) of compound **9** showed that the HOMO was located on the anthryl moiety and that the LUMO involved the anthryl–Bpin part. This result matched with an ICT from the aromatic π system to the electron-deficient boron center. Again, as for compound **2**, the binding of F^- quenched all of the transitions in which the LUMO was involved. The fine-structure and spectral position of the evolving band at about 420 nm pointed to emission from the LE π,π* state of the anthracene chromophore itself.

For some representative cases (compounds **2**, **4**, **6**, and **9**) their interactions with other anions (Cl^-, Br^-, CN^-, NO_3^-, CH_3COO^-, and $H_2PO_4^-$) were also investigated. However, with the exception of cyano-substituted compound **2**, which showed fluorescence quenching upon the addition of 60 equivalents of CN^- (27% quenching) or $H_2PO_4^-$ (60% quenching), no alteration of the fluorescence properties was observed. Hence, these compounds showed a very selective response to fluoride ions.

As described above for the addition of TFA, it was of interest to verify the possibility of observing fluorescence modulation by the addition of fluoride (60 equiv) to representative compounds (**6** and **9**) in a water-containing medium (MeCN/water, 1:1). Although the degree of fluorescence quenching was lower, it was possible to observe a significant effect, that is, 14 and 22% quenching for compounds **6** and **9**, respectively. The Lewis basicity of fluoride is counterbalanced by the formation of hydrogen-bonding interactions with surrounding water molecules and, thus, within this scenario, our observations are gratifying. However, for a clear on-off fluorescence response, it is desirable to keep the presence of water to a minimum.

Conclusion

A series of borylated arylisoquinolines was prepared and their photophysical properties were investigated. The emission properties of these compounds were fine-tuned by variation of the aryl moiety and its electron-withdrawing or electron-donating substitution pattern. On the one hand, compounds with aryl moieties that were harder to oxidize

showed emission maxima in the blue-shifted spectral region (for example cyano-substituted compound **2** at $\lambda_{max}=$ 437 nm), whereas, on the other hand, compounds **6** and **9**, which contained the easiest-to-oxidize aryl residues, showed LW emission maxima at $\lambda_{max}=608$ and 571 nm, respectively. These ICT phenomena, which were implicated in the excited-state behavior, were further corroborated by the observation of significant solvatochromic effects and have been characterized by DFT calculations. An analysis of the frontier orbitals of the optimized molecular geometries (at the B3LYP/6-31+G(d,p) level of theory) of the naphthalene-derived compounds showed that ICT proceeded from the aryl residue to the isoquinoline part of the molecule (except for compound **2**). The general importance of boron substitution for the described photophysical phenomena became obvious by including the non-borylated arylisoquinolines for the sake of comparison. In general, their maximum emission wavelengths were strongly blue-shifted and the quantum yields were drastically decreased.

The molecular design of the title compounds enabled the dual switching of their emission properties by the addition of an acid (protonation at the isoquinoline N atom) or fluoride ions (fluoroboronate formation with the Bpin moiety). As a general trend, protonation caused significant fluorescence enhancement for compounds with weak ICT character (compounds **1** and **2**) and strong quenching for compounds with pronounced ICT character (compounds **5**–**9**). On the addition of fluoride, almost quantitative emission quenching was observed, which, in the case of compound **9**, was accompanied by the build-up of a blue-shifted emission, thus resulting in a ratiometric response. Hence, these borylated arylisoquinolines not only constitute an interesting new class of fluorophores, but they also possess potential as ion-triggered molecular switches. Their potential applications may include fluoride sensing in non-aqueous media or the use as fluorescent tags with tunable emission color. In particular, compound **6** and its derivatives are of interest because of its strongly red-shifted emission signature and significant quantum yields.

Experimental Section

Materials and methods: ^{1}H NMR spectra were recorded at 300, 400, or 500 MHz and ^{13}C NMR spectra were recorded at 75, 100, or 125 MHz, with the solvent peak used as an internal reference ($CDCl_3$: $\delta=7.26$ and 77.0 ppm for ^{1}H and ^{13}C, respectively); ^{11}B NMR spectra were recorded with complete proton decoupling at 160 MHz by using $BF_3{\cdot}Et_2O$ as a standard ($\delta=0.00$ ppm for ^{11}B NMR). ^{19}F NMR spectra were recorded with complete proton decoupling at 377 MHz by using trichlorofluoromethane as a standard ($\delta=0.00$ ppm for ^{19}F NMR). Column chromatography was performed on silica gel (Merck Kieselgel 60). Analytical thin layer chromatography was performed on aluminum-backed plates (1.5×5.0 cm) that were pre-coated (0.25 mm) with silica gel (Merck, Silica Gel 60 F_{254}). The compounds were visualized by exposure to UV light or by dipping the plates in a solution of 5% $(NH_4)_2Mo_7O_{24}{\cdot}4H_2O$ in EtOH (95%, w/v), followed by heating. MeCN (Scharlab) was of spectroscopic grade. Trifluoroacetic acid (TFA) was purchased from Aldrich. The different anions were applied as their tetra-*n*-butylammonium salts (Bu_4NX; X=Cl, Br, CH_3COO, NO_3, H_2PO_4, CN; $Bu_4NF{\cdot}3H_2O$), which were purchased from Aldrich in the highest available quality. The metal cations were used in the form of their perchlorates (highest available quality from Aldrich; $NaClO_4$, $AgClO_4$, $Mg(ClO_4)_2$, $Pb(ClO_4)_2{\cdot}3H_2O$, $Zn(ClO_4)_2{\cdot}6H_2O$).

All of the reactions were performed in oven-dried Schlenk tubes under an argon atmosphere by employing standard techniques. Anhydrous THF was obtained by using Grubbs-type anhydrous solvent drying columns. Anhydrous 1,4-dioxane was obtained by distillation from sodium by using benzophenone as an indicator. EtOAc, MeOH, *n*-hexane, and toluene were purchased from Carlo Erba. Bis(pinacolato)diboron (B_2pin_2) and pinacolborane (HBpin) were purchased from Alfa Aesar and Aldrich, respectively, and used without further purification. [{Ir(μ-OMe)(cod)}$_2$] (cod=1,5-cyclooctadiene), Sphos ligand, [$Pd_2(dba)_3$] (dba=dibenzylideneacetone), and [$Pd(PPh_3)_4$] were purchased from Strem and used without further purification. 1-Chloroisoquinoline was purchased from Aldrich. Products **1**, **4**, **7**, and **8** and their corresponding non-borylated models (**M1**, **M4**, **M7**, **M8**) were prepared according to literature procedures.[45]

All photophysical measurements were performed on air-equilibrated solutions in MeCN at RT (typically adjusting an optical density of 0.1–0.2 at the excitation wavelength), by using quartz cuvettes with a 1 cm optical path length. UV/Vis absorption spectra were recorded on a UV-1603 spectrophotometer (Shimadzu). Fluorescence spectra were recorded on a Cary Eclipse fluorimeter (Varian) and corrected for the spectroscopic response of the setup. To record the fluorescence spectra of the compounds in the absence of additives, the samples were excited at the UV/Vis absorption maximum. The fluorescence quantum yields (error ±25%) were determined by using quinine sulfate ($\Phi_f=0.55$ in 0.05 M sulfuric acid)[65] as a reference and corrected for the difference between the refractive indices of water and MeCN.[30] The excitation wavelengths for the fluorescence measurements on the addition of TFA or Bu_4NF were chosen to coincide with the isosbestic points of the UV/Vis absorption titration spectra. Lifetime measurements were performed by means of time-correlated single-photon-counting (Edinburgh instruments FLS 920) with picosecond pulsed EPLEDs (EPLED 280, EPLED 330, EPLED 340, or EPLED 360) for excitation close to the respective absorption maximum. Deconvolution analysis of the decay curves yielded the corresponding fluorescence lifetimes. For this purpose, the instrument-response function was recorded by using a light-scattering Ludox solution.

DFT calculations: All calculations were performed by using the Gaussian03 program.[66] The ground-state geometries were calculated by applying the Kohn–Sham density functional theory (DFT) with the Becke3 Lee–Yang–Parr hybrid functional (B3LYP) method by using the 6-31+G(d,p) basis set for the full structural optimization and frequency calculations. Analytical frequency calculations were performed to verify the stationary points on the potential-energy surface. To calculate the frontier orbital energies, time-dependent density functional theory (TD-DFT) was applied at the B3LYP/6-31+G(d,p) level of theory.

General procedure for the synthesis of models M2, M3, M5, M6, and M9: According to a literature procedure,[49] a pre-dried Schlenk tube was charged with [$Pd_2(dba)_3$] (11 mg, 0.012 mmol), SPhos (39 mg, 0.096 mmol), B_2pin_2 (305 mg, 1.2 mmol), the haloarene (254 mg, 1.2 mmol), and potassium acetate (196 mg, 2.00 mmol). After three cycles of vacuum/argon-flushing, anhydrous 1,4-dioxane (4.0 mL) was added through the septum with a syringe. The reaction mixture was heated at 110 °C for 5 h. At this point, a solution of 1-chloroisoquinoline (1.0 mmol, 163 mg) in 1,4-dioxane (1.0 mL) and an aqueous solution of K_3PO_4 (5 M, 1.0 mL) were added by syringe into the reaction flask. Then, the reaction mixture was heated at 110 °C for a further 4 h, before being cooled to RT and diluted with water (10 mL) and EtOAc (10 mL). The organic phase was separated and the aqueous phase was extracted with EtOAc (3×10 mL). The combined organic phases were dried over anhydrous $MgSO_4$, filtered, and concentrated to dryness. The products were purified by flash chromatography on silica gel (*n*-hexane/EtOAc).

*4-(Isoquinolin-1-yl)-1-naphthonitrile (**M2**)*: According to the general procedure, starting from 4-bromo-1-naphthonitrile[67] (290 mg, 1.25 mmol); flash chromatography on silica gel (*n*-hexane/EtOAc, 4:1) gave compound **M2** (134 mg, 48% yield) as a brown solid. M.p. 115–117 °C;

^{1}H NMR (500 MHz, $CDCl_3$): δ = 8.71 (d, J = 5.5 Hz, 1H; Ar-H), 8.37 (d, J = 8.5 Hz, 1H; Ar-H), 8.07 (d, J = 7.5 Hz, 1H; Ar-H), 7.98 (d, J = 8.5 Hz, 1H; Ar-H), 7.83 (d, J = 5.5 Hz, 1H; Ar-H), 7.75–7.70 (m, 2H; Ar-H), 7.65 (d, J = 7.5 Hz, 1H; Ar-H), 7.51 (d, J = 8.5 Hz, 1H; Ar-H), 7.48–7.44 ppm (m, 3H; Ar-H); ^{13}C NMR (125 MHz, $CDCl_3$): δ = 162.4 (C), 158.4 (C), 142.2 (CH), 136.4 (C), 132.6 (C), 132.0 (C), 131.8 (CH), 130.5 (CH), 128.6 (CH), 127.9 (CH), 127.7 (C), 127.6 (CH), 127.0 (CH), 126.9 (CH), 126.8 (CH), 126.6 (CH), 125.5 CH), 120.9 (CH), 117.7 (C), 110.8 ppm (CN); HRMS (EI): m/z calcd for $C_{20}H_{11}N_2$: 279.0922 $[M-1]^+$; found: 279.0913; elemental analysis calcd (%) for $C_{20}H_{12}N_2$: C 85.69, H, 4.31, N, 9.99; found: C 85.74, H, 4.28, N, 9.80.

*1-(4-Fluoronaphthalen-1-yl)isoquinoline (**M3**)*: According to the general procedure, starting from 1-bromo-4-fluoronaphthalene[68] (515 mg, 2.3 mmol); flash chromatography on silica gel (*n*-hexane/EtOAc, 6:1) gave compound **M3** (350 mg, 67% yield) as a colorless solid. M.p. 108–110 °C; ^{1}H NMR (400 MHz, $CDCl_3$): δ = 8.73 (d, J = 5.6 Hz, 1H; Ar-H), 8.25 (d, J = 8.3 Hz, 1H; Ar-H), 7.97 (d, J = 8.1 Hz, 1H; Ar-H), 7.79 (d, J = 5.6 Hz, 1H; Ar-H), 7.72 (t, J = 7.4 Hz, 1H; Ar-H), 7.64 (d, J = 8.3 Hz, 1H; Ar-H), 7.60–7.52 (m, 2H; Ar-H), 7.47–7.38 (m, 3H; Ar-H), 7.32 ppm (dd, J(H,F) = 9.8 Hz, J = 8.1 Hz, 1H; Ar-H); ^{13}C NMR (100 MHz, $CDCl_3$): δ = 159.7 (C), 159.1 (d, ^1J(C,F) = 251 Hz; C), 142.4 (CH), 136.5 (C), 133.7 (d, J(C,F) = 4 Hz; C), 133.1 (d, J(C,F) = 4 Hz; C), 130.3 (CH), 128.4 (C), 127.7 (CH), 127.6 (CH), 127.3 (CH), 127.0 (CH), 126.3 (CH), 126.0 (CH), 123.9 (d, ^2J(C,F) = 16 Hz; C), 120.8 (d, ^3J(C,F) = 5 Hz; CH), 120.4 (CH), 108.9 ppm (d, ^2J(C,F) = 20 Hz; CH); ^{19}F NMR (377 MHz, $CDCl_3$): δ = −122.0 ppm; HRMS (EI): m/z calcd for $C_{19}H_{11}FN$: 272.0876 $[M-1]^+$; found: 272.0884; elemental analysis calcd (%) for $C_{19}H_{12}FN$: C 83.50, H 4.43, N 5.12; found: C 83.70, H 4.55, N 5.22.

*1-(8-Methoxynaphthalen-1-yl)isoquinoline (**M5**)*: According to the general procedure, starting from 1-bromo-4-methoxynaphthalene[69] (564 mg, 2.4 mmol); flash chromatography on silica gel (*n*-hexane/EtOAc, 4:1→2:1) gave compound **M5** (228 mg, 40% yield) as a light-yellow solid. M.p. 152–154 °C; ^{1}H NMR (500 MHz, $CDCl_3$): δ = 8.70 (d, J = 5.7 Hz, 1H; Ar-H), 8.39 (d, J = 8.4 Hz, 1H; Ar-H), 7.91 (d, J = 8.4 Hz, 1H; Ar-H), 7.73 (d, J = 5.7 Hz, 1H; Ar-H), 7.69–7.66 (m, 2H; Ar-H), 7.51 (d, J = 7.8 Hz, 1H; Ar-H), 7.48 (td, J = 7.6, 1.1 Hz, 1H; Ar-H), 7.42–7.39 (m, 2H; Ar-H), 7.34 (td, J = 7.8, 1.1 Hz, 1H; Ar-H), 6.96 (d, J = 7.8 Hz, 1H; Ar-H), 4.10 ppm (s, 3H; OCH_3); ^{13}C NMR (125 MHz, $CDCl_3$): δ = 160.6 (C), 155.9 (C), 142.4 (CH), 136.5 (C), 133.2 (C), 130.1 (CH), 129.4 (C), 128.5 (C), 128.0 (CH), 127.9 (CH), 127.0 (CH), 126.8 (CH), 126.7 (CH), 125.7 (CH), 125.6 (C), 125.2 (CH), 122.1 (CH), 119.9 (CH), 103.2 (CH), 55.6 ppm (OCH_3); HRMS (EI): m/z calcd for $C_{20}H_{14}NO$: 284.1075 $[M-1]^+$; found: 284.1079; elemental analysis calcd (%) for $C_{20}H_{15}NO$: C 84.19, H 5.30, N 4.91; found: C 84.15, H 5.52, N 4.95.

*4-(Isoquinolin-1-yl)-N,N-dimethylnaphthalen-1-amine (**M6**)*: According to the general procedure, starting from 4-bromo-*N*,*N*-dimethylnaphthalen-1-amine[70] (300 mg, 1.2 mmol); flash chromatography on silica gel (*n*-hexane/EtOAc, 5:1) gave compound **M6** (163 mg, 55% yield) as a viscous orange/yellow oil. ^{1}H NMR (300 MHz, $CDCl_3$): δ = 8.68 (d, J = 5.7 Hz, 1H; Ar-H), 8.33 (d, J = 8.6 Hz, 1H; Ar-H), 7.91 (d, J = 8.3 Hz, 1H; Ar-H), 7.73 (d, J = 5.7 Hz, 1H; Ar-H), 7.72–7.64 (m, 2H; Ar-H), 7.50–7.38 (m, 4H; Ar-H), 7.32–7.27 (m, 1H; Ar-H), 7.19 (d, J = 7.7 Hz, 1H; Ar-H), 2.98 ppm (s, 6H; $N(CH_3)_2$); ^{13}C NMR (75 MHz, $CDCl_3$): δ = 160.8 (C), 151.6 (C), 142.2 (CH), 136.5 (C), 133.6 (C), 131.4 (C), 130.2 (CH), 128.8 (C), 128.4 (C), 128.0 (CH), 127.8 (CH), 127.1 (CH), 126.8 (CH), 126.4 (CH), 126.1 (CH), 125.1 (CH), 124.4 (CH), 120.0 (CH), 113.2 (CH), 45.2 ppm ($N(CH_3)_2$); HRMS (EI): m/z calcd for $C_{21}H_{17}N_2$: 297.1392 $[M-1]^+$; found: 297.1381; elemental analysis calcd (%) for $C_{21}H_{18}N_2$: C 84.53, H 6.08, N 9.39; found: C 84.70, H 6.15, N 9.35.

*1-(Anthracen-1-yl)isoquinoline (**M9**)*: According to the general procedure, starting from 1-chloroanthracene[71] (254 mg, 1.2 mmol); flash chromatography on silica gel (*n*-hexane/EtOAc 4:1) gave compound **M9** (223 mg, 73% yield) as a yellow solid. M.p. 120–122 °C; ^{1}H NMR (500 MHz, $CDCl_3$): δ = 8.76 (d, J = 5.5 Hz, 1H; Ar-H), 8.54 (s, 1H; Ar-H), 8.17 (d, J = 8.5 Hz, 1H; Ar-H), 8.01 (d, J = 8.5 Hz, 1H; Ar-H), 7.97 (s, 1H; Ar-H), 7.96 (d, J = 7.0 Hz, 1H; Ar-H), 7.81 (d, J = 6.0 Hz, 1H; Ar-H), 7.70–7.66 (m, 3H; Ar-H), 7.61 (t, J = 8.5 Hz, 1H; Ar-H), 7.58 (d, J = 8.5 Hz, 1H; Ar-H), 7.43 (t, J = 7.5 Hz, 1H; Ar-H), 7.38 (t, J = 8.5 Hz, 1H; Ar-H), 7.34 ppm (t, J = 8.5 Hz, 1H; Ar-H); ^{13}C NMR (125 MHz, $CDCl_3$): δ = 160.5 (C), 142.4 (CH), 137.0 (C), 136.5 (C), 131.8 (C), 131.8 (C), 131.5 (C), 130.7 (C), 130.2 (CH), 129.1 (CH), 128.5 (CH), 128.3 (C), 127.8 (CH), 127.7 (CH), 127.2 (CH), 127.2 (CH), 126.8 (CH), 126.6 (CH), 125.5 (CH), 125.3 (CH), 124.9 (CH), 124.6 (CH), 120.3 ppm (CH); HRMS (EI): m/z calcd for $C_{23}H_{15}N$: 305.1204 $[M]^+$; found: 305.1200; elemental analysis calcd (%) for $C_{23}H_{15}N$: C 90.46, H 4.95, N 4.59; found: C 90.52, H 5.08, N 4.44.

General procedure for the Ir-catalyzed borylation reactions: Following a recently reported method,[45] a pre-dried Schlenk tube was charged with the substrate (**M2**, **M3**, **M5**, **M6**, or **M9**) and B_2Pin_2 (1 equiv). After three cycles of vacuum/argon-flushing, the catalyst stock solution[72] (1 mL per 0.5 mmol substrate) and HBPin (5% mol) were added and the reaction mixture was stirred at 55–80 °C until the starting material had been completely consumed (by TLC). The mixture was cooled to RT, concentrated to dryness, and purified by column chromatography on silica gel (*n*-hexane/EtOAc or toluene/EtOAc).

*4-(Isoquinolin-1-yl)-3-(4,4,5,5-tetramethyl-1,3,2-dioxaborolan-2-yl)-1-naphthonitrile (**2**)*: According to the general procedure, starting from compound **M2** (90 mg, 0.32 mmol); flash chromatography on silica gel (toluene/EtOAc, 7:1) gave compound **2** (82 mg, 63% yield) as a light-brown solid. M.p. 149–151 °C; ^{1}H NMR (500 MHz, $CDCl_3$): δ = 8.67 (d, J = 6.0 Hz, 1H; Ar-H), 8.42 (s, 1H; Ar-H), 8.34 (d, J = 8.0 Hz, 1H; Ar-H), 7.93 (d, J = 8.0 Hz, 1H; Ar-H), 7.79 (d, J = 6.0 Hz, 1H; Ar-H), 7.71 (t, J = 8.0 Hz, 1H; Ar-H), 7.67 (t, J = 8.0 Hz, 1H; Ar-H), 7.45–7.36 (m, 3H; Ar-H), 7.32 (d, J = 7.5 Hz, 1H; Ar-H), 0.95 (s, 6H; 2×CH_3), 0.76 ppm (s, 6H; 2×CH_3); ^{13}C NMR (75 MHz, $CDCl_3$): δ = 159.6 (C), 141.6 (C), 137.5 (CH), 136.0 (C), 133.5 (C), 131.9 (C), 130.1 (C), 129.3 (CH), 129.0 (C), 127.7 (CH), 127.6 (CH), 127.1 (CH), 126.8 (CH), 126.6 (CH), 125.2 (CH), 120.2 (CH), 117.8 (CH), 110.0 (CN), 83.7 (2×C), 24.3 (2×CH_3), 24.0 ppm (2×CH_3), (*C*-B not observed); ^{11}B NMR (160 MHz, $CDCl_3$): δ = 31.0 ppm (br s); HRMS (EI): m/z calcd for $C_{26}H_{23}BN_2O_2$: 406.1853 $[M]^+$; found: 406.1840; elemental analysis calcd (%) for $C_{26}H_{23}BN_2O_2$: C 76.86, H 5.71, N 6.90; found: C 77.00, H 5.65, N 6.78.

*1-(4-Fluoro-2-(4,4,5,5-tetramethyl-1,3,2-dioxaborolan-2-yl)naphthalen-1-yl)isoquinoline (**3**)*: According to the general procedure, starting from compound **M3** (137 mg, 0.5 mmol); flash chromatography on silica gel (toluene/EtOAc, 3:1) gave compound **3** (134 mg, 67% yield) as a viscous light-yellow oil. ^{1}H NMR (400 MHz, $CDCl_3$): δ = 8.65 (d, J = 5.8 Hz, 1H; Ar-H), 8.20 (d, J = 8.4 Hz, 1H; Ar-H), 7.89 (d, J = 8.2 Hz, 1H; Ar-H), 7.73 (d, J = 5.8 Hz, 1H; Ar-H), 7.65–7.61 (m, 2H; Ar-H), 7.56 (t, J = 7.6 Hz, 1H; Ar-H), 7.42–7.31 (m, 4H; Ar-H), 0.94 (s, 6H; 2×CH_3), 0.74 ppm (s, 6H; 2×CH_3); ^{13}C NMR (100 MHz, $CDCl_3$): δ = 160.9 (C), 158.2 (d, ^1J(C,F) = 251 Hz, C), 141.9 (CH), 140.2 (d, ^4J(C,F) = 3 Hz; C), 136.0 (C), 133.9 (d, ^3J(C,F) = 4 Hz; C), 129.7 (CH), 127.3 (CH), 127.0 (CH), 127.0 (CH), 126.8 (CH), 126.5 (CH), 125.0 (d, ^2J(C,F) = 17 Hz; C), 120.4 (d, ^3J(C,F) = 5 Hz; CH), 119.7 (CH), 113.4 (d, ^2J(C,F) = 18 Hz; CH), 83.4 (2×C), 24.4 (2×CH_3), 24.1 ppm (2×CH_3), (*C*-B not observed); ^{11}B NMR (128 MHz, $CDCl_3$): δ = 30.3 ppm (br s); ^{19}F NMR (377 MHz, $CDCl_3$): δ = −124.3 ppm; HRMS (EI): m/z calcd for $C_{25}H_{23}BFNO_2$: 399.1806 $[M]^+$; found: 399.1807; elemental analysis calcd (%) for $C_{25}H_{23}BFNO_2$: C 75.21, H 5.81, N 3.51; found: C 75.38, H 5.88, N 3.40.

*1-(8-Methoxy-2-(4,4,5,5-tetramethyl-1,3,2-dioxaborolan-2-yl)naphthalen-1-yl)isoquinoline (**5**)*: According to the general procedure, starting from compound **M5** (143 mg, 0.5 mmol); flash chromatography on silica gel (*n*-hexane/EtOAc, 2:1) gave compound **5** (175 mg, 85% yield) as a yellow solid. M.p. 154–156 °C; ^{1}H NMR (500 MHz, $CDCl_3$): δ = 8.64 (d, J = 5.8 Hz, 1H; Ar-H), 8.34 (d, J = 8.5 Hz, 1H; Ar-H), 7.85 (d, J = 8.2 Hz, 1H; Ar-H), 7.68 (d, J = 5.8 Hz, 1H; Ar-H), 7.59 (t, J = 7.5 Hz, 1H; Ar-H), 7.46 (t, J = 8.5 Hz, 1H; Ar-H), 7.44 (d, J = 8.2 Hz, 1H; Ar-H), 7.31–7.24 (m, 4H; Ar-H), 4.11 (s, 3H; OCH_3), 0.92 (s, 6H; 2×CH_3), 0.74 ppm (s, 6H; 2×CH_3); ^{13}C NMR (125 MHz, $CDCl_3$): δ = 161.9 (C), 154.6 (C), 141.9 (CH), 136.9 (C), 135.9 (C), 133.3 (C), 129.9 (C), 129.5 (CH), 127.6 (CH), 126.8 (C), 126.5 (CH), 126.5 (CH), 126.4 (CH), 126.3 (CH), 125.9 (CH), 121.8 (CH), 119.3 (CH), 107.6 (CH), 83.1 (2×C), 55.6 (OCH_3), 24.3 (2×CH_3), 24.1 ppm (2×CH_3), (*C*-B not observed); ^{11}B NMR (160 MHz, $CDCl_3$): δ = 31.2 ppm (br s); HRMS (EI): m/z calcd for $C_{26}H_{26}BNO_3$: 411.2006 $[M]^+$; found: 411.1998; elemental analysis calcd

(%) for $C_{26}H_{26}BNO_3$: C 75.92, H 6.37, N 3.41; found: C 76.10, H 6.32, N 3.53.

*4-(Isoquinolin-1-yl)-N,N-dimethyl-3-(4,4,5,5-tetramethyl-1,3,2-dioxaborolan-2-yl)naphthalen-1-amine (**6**)*: According to the general procedure, starting from compound **M6** (149 mg, 0.5 mmol); flash chromatography on silica gel (*n*-hexanes/EtOAc, 2:1) gave compound **6** (182 mg, 86% yield) as an orange solid. M.p. 166–168 °C; ^{1}H NMR (500 MHz, $CDCl_3$): $\delta = 8.64$ (d, $J = 5.5$ Hz, 1H; Ar-H), 8.33 (d, $J = 8.5$ Hz, 1H; Ar-H), 7.87 (d, $J = 8.0$ Hz, 1H; Ar-H), 7.70 (d, $J = 5.5$ Hz, 1H; Ar-H), 7.61 (t, $J = 8.0$ Hz, 1H; Ar-H), 7.52 (s, 1H; Ar-H), 7.50–7.48 (m, 2H; Ar-H), 7.33 (t, $J = 8.0$ Hz, 1H; Ar-H), 7.30–7.25 (m, 2H; Ar-H), 2.99 (s, 6H; $N(CH_3)_2$), 0.93 (s, 6H; $2\times CH_3$), 0.75 ppm (s, 6H; $2\times CH_3$); ^{13}C NMR (125 MHz, $CDCl_3$): $\delta = 162.2$ (C), 150.2 (C), 142.0 (CH), 139.2 (C), 136.0 (C), 133.6 (C), 130.2 (C), 129.9 (C), 129.7 (CH), 127.8 (CH), 127.3 (CH), 126.6 (CH), 126.4 (CH), 126.0 (CH), 125.8 (CH), 124.1 (CH), 119.3 (CH), 118.1 (CH), 83.1 ($2\times$C), 45.3 ($N(CH_3)_2$), 24.4 ($2\times CH_3$), 24.2 ppm ($2\times CH_3$), (*C*-B not observed); ^{11}B NMR (160 MHz, $CDCl_3$): $\delta = 31.4$ ppm (br s); HRMS (EI): *m/z* calcd for $C_{27}H_{29}BN_2O_2$: 424.2322 $[M]^+$; found: 424.2315; elemental analysis calcd (%) for $C_{27}H_{29}BN_2O_2$: C 76.42, H 6.89, N 6.60; found: C 76.52, H 7.00, N 6.68.

*1-(2-(4,4,5,5-Tetramethyl-1,3,2-dioxaborolan-2-yl)anthracen-1-yl)isoquinoline (**9**)*: According to the general procedure, starting from compound **M9** (153 mg, 0.5 mmol); flash chromatography on silica gel (*n*-hexane/EtOAc, 2:1) gave compound **9** (205 mg, 95% yield) as a light-brown solid. M.p. 170–172 °C; ^{1}H NMR (500 MHz, $CDCl_3$): $\delta = 8.73$ (d, $J = 5.7$ Hz, 1H; Ar-H), 8.50 (s, 1H; Ar-H), 8.13 (d, $J = 8.5$ Hz, 1H; Ar-H), 7.99 (d, $J = 8.6$ Hz, 1H; Ar-H), 7.95–7.88 (m, 3H; Ar-H), 7.79 (d, $J = 5.8$ Hz, 1H; Ar-H), 7.68 (d, $J = 8.6$ Hz, 1H; Ar-H), 7.63 (t, $J = 8.2$ Hz, 1H; Ar-H), 7.46 (d, $J = 8.5$ Hz, 1H; Ar-H), 7.42 (t, $J = 7.7$ Hz, 1H; Ar-H), 7.32 (d, $J = 7.5$ Hz, 1H; Ar-H), 7.29 (d, $J = 7.5$ Hz, 1H; Ar-H), 0.96 (s, 6H; $2\times CH_3$), 0.76 ppm (s, 6H; $2\times CH_3$); ^{13}C NMR (125 MHz, $CDCl_3$): $\delta = 161.7$ (C), 145.0 (C), 142.0 (CH), 136.1 (C), 132.7 (C), 132.1 (C), 131.7 (C), 130.8 (C), 129.8 (C), 129.7 (CH), 129.2 (CH), 128.8 (CH), 127.8 (CH), 127.7 (CH), 127.5 (CH), 126.7 (CH), 126.5 (CH), 126.3 (CH), 126.2 (CH), 125.9 (CH), 125.1 (CH), 119.7 (CH), 83.2 ($2\times$C), 24.4 ($2\times CH_3$), 24.1 ppm ($2\times CH_3$), (*C*-B not observed); ^{11}B NMR (160 MHz, $CDCl_3$): $\delta = 31.2$ ppm (br s); HRMS (EI): *m/z* calcd for $C_{29}H_{26}BNO_2$: 431.2057 $[M]^+$; found: 431.2060; elemental analysis calcd (%) for $C_{29}H_{26}BNO_2$: C 80.75, H 6.08, N 3.25; found: C 80.83, H 6.12, N 3.18.

Acknowledgements

Financial support by MINECO, Madrid (CTQ2011-28390 to U.P. and CTQ2010-15297 and CTQ2010-14974 to A.R.), the European FEDER funds, and the Junta de Andalucía (2008/FQM-3685 to U.P. and 2008/FQM-3833 and 2009/FQM-4537 to A.R.) is gratefully acknowledged. A.R. thanks the European Union for a Marie Curie Reintegration Grant (FP7-PEOPLE-2009-RG-256461) and the Consejo Superior de Investigaciones Científicas (CSIC, Madrid) for a JAE-Doc Fellowship. H.S.E.-S. thanks the Computational Laboratory for Analysis, Modeling, and Visualization at the Jacobs University Bremen (Germany) for computing time.

[1] C. D. Entwistle, T. B. Marder, *Angew. Chem.* **2002**, *114*, 3051; *Angew. Chem. Int. Ed.* **2002**, *41*, 2927.
[2] C. D. Entwistle, T. B. Marder, *Chem. Mater.* **2004**, *16*, 4574.
[3] K. Parab, K. Venkatasubbaiah, F. Jäkle, *J. Am. Chem. Soc.* **2006**, *128*, 12879.
[4] Y. Qin, I. Kiburu, S. Shah, F. Jäkle, *Macromolecules* **2006**, *39*, 9041.
[5] M. Elbing, G. C. Bazan, *Angew. Chem.* **2008**, *120*, 846; *Angew. Chem. Int. Ed.* **2008**, *47*, 834.
[6] H. Li, F. Jäkle, *Angew. Chem.* **2009**, *121*, 2349; *Angew. Chem. Int. Ed.* **2009**, *48*, 2313.
[7] Z.-Q. Liu, M. Shi, F.-Y. Li, Q. Fang, Z.-H. Chen, T. Yi, C.-H. Huang, *Org. Lett.* **2005**, *7*, 5481.
[8] J. C. Collings, S.-Y. Poon, C. Le Droumaguet, M. Charlot, C. Katan, L.-O. Pålsson, A. Beeby, J. A. Mosely, H. M. Kaiser, D. Kaufmann, W.-Y. Wong, M. Blanchard-Desce, T. B. Marder, *Chem. Eur. J.* **2009**, *15*, 198.
[9] R. Stahl, C. Lambert, C. Kaiser, R. Wortmann, R. Jakober, *Chem. Eur. J.* **2006**, *12*, 2358.
[10] H. C. Schmidt, L. G. Reuter, J. Hamacek, O. S. Wenger, *J. Org. Chem.* **2011**, *76*, 9081.
[11] T. W. Hudnall, C.-W. Chiu, F. P. Gabbaï, *Acc. Chem. Res.* **2009**, *42*, 388.
[12] Z. M. Hudson, S. Wang, *Acc. Chem. Res.* **2009**, *42*, 1584.
[13] C. R. Wade, A. E. J. Broomsgrove, S. Aldridge, F. P. Gabbaï, *Chem. Rev.* **2010**, *110*, 3958.
[14] Z. Guo, I. Shin, J. Yoon, *Chem. Commun.* **2012**, *48*, 5956.
[15] R. Martínez-Máñez, F. Sancenón, *Chem. Rev.* **2003**, *103*, 4419.
[16] T. W. Hudnall, F. P. Gabbaï, *J. Am. Chem. Soc.* **2007**, *129*, 11978.
[17] M. H. Lee, T. Agou, J. Kobayashi, T. Kawashima, F. P. Gabbaï, *Chem. Commun.* **2007**, 1133.
[18] Y. Kubo, A. Kobayashi, T. Ishida, Y. Misawa, T. D. James, *Chem. Commun.* **2005**, 2846.
[19] K. M. K. Swamy, Y. J. Lee, H. N. Lee, J. Chun, Y. Kim, S.-J. Kim, J. Yoon, *J. Org. Chem.* **2006**, *71*, 8626.
[20] G. Zhou, M. Baumgarten, K. Müllen, *J. Am. Chem. Soc.* **2008**, *130*, 12477.
[21] S. Yamaguchi, T. Shirasaka, S. Akiyama, K. Tamao, *J. Am. Chem. Soc.* **2002**, *124*, 8816.
[22] Y. Kubo, M. Yamamoto, M. Ikeda, M. Takeuchi, S. Shinkai, S. Yamaguchi, K. Tamao, *Angew. Chem.* **2003**, *115*, 2082; *Angew. Chem. Int. Ed.* **2003**, *42*, 2036.
[23] X. Y. Liu, D. R. Bai, S. Wang, *Angew. Chem.* **2006**, *118*, 5601; *Angew. Chem. Int. Ed.* **2006**, *45*, 5475.
[24] D.-R. Bai, X.-Y. Liu, S. Wang, *Chem. Eur. J.* **2007**, *13*, 5713.
[25] M.-S. Yuan, Z.-Q. Liu, Q. Fang, *J. Org. Chem.* **2007**, *72*, 7915.
[26] Y. Sun, S. Wang, *Inorg. Chem.* **2009**, *48*, 3755.
[27] Z. C. Xu, S. K. Kim, S. J. Han, C. Lee, G. Kociok-Kohn, T. D. James, J. Yoon, *Eur. J. Org. Chem.* **2009**, 3058.
[28] H. Pan, G.-L. Fu, Y.-H. Zhao, C.-H. Zhao, *Org. Lett.* **2011**, *13*, 4830.
[29] A. P. de Silva, T. P. Vance, M. E. S. West, G. D. Wright, *Org. Biomol. Chem.* **2008**, *6*, 2468.
[30] B. Valeur, *Molecular Fluorescence: Principles and Applications*, 1st ed., Wiley-VCH, Weinheim, **2001**.
[31] A. P. de Silva, H. Q. N. Gunaratne, T. Gunnlaugsson, A. J. M. Huxley, C. P. McCoy, J. T. Rademacher, T. E. Rice, *Chem. Rev.* **1997**, *97*, 1515.
[32] Y. Kim, H.-S. Huh, M. H. Lee, I. L. Lenov, H. Zhao, F. P. Gabbaï, *Chem. Eur. J.* **2011**, *17*, 2057.
[33] Z. M. Hudson, X.-Y. Liu, S. Wang, *Org. Lett.* **2011**, *13*, 300.
[34] M. M. M. Raposo, B. García-Acosta, T. Ábalos, P. Calero, R. Martínez-Máñez, J. V. Ros-Lis, J. Soto, *J. Org. Chem.* **2010**, *75*, 2922.
[35] E. B. Veale, T. Gunnlaugsson, *J. Org. Chem.* **2008**, *73*, 8073.
[36] M. Kluciar, R. Ferreira, B. de Castro, U. Pischel, *J. Org. Chem.* **2008**, *73*, 6079.
[37] B. Liu, H. Tian, *J. Chem. Mater.* **2005**, *17*, 2681.
[38] D. Esteban-Gómez, L. Fabbrizzi, M. Licchelli, *J. Org. Chem.* **2005**, *70*, 5717.
[39] D. Curiel, A. Cowley, P. D. Beer, *Chem. Commun.* **2005**, 236.
[40] C. Bohne, H. Ihmels, M. Waidelich, C. Yihwa, *J. Am. Chem. Soc.* **2005**, *127*, 17158.
[41] D. Aldakov, M. A. Palacios, P. Anzenbacher Jr., *Chem. Mater.* **2005**, *17*, 5238.
[42] T. Gunnlaugsson, P. E. Kruger, T. C. Lee, R. Parkesh, F. M. Pfeffer, G. M. Hussey, *Tetrahedron Lett.* **2003**, *44*, 6575.
[43] E. J. Cho, J. W. Moon, S. W. Ko, J. Y. Lee, S. K. Kim, J. Yoon, K. C. Nam, *J. Am. Chem. Soc.* **2003**, *125*, 12376.
[44] S. K. Kim, J. Yoon, *Chem. Commun.* **2002**, 770.
[45] A. Ros, B. Estepa, R. López-Rodríguez, E. Álvarez, R. Fernández, J. M. Lassaletta, *Angew. Chem.* **2011**, *123*, 11928; *Angew. Chem. Int. Ed.* **2011**, *50*, 11724.
[46] R. Ferreira, P. Remón, U. Pischel, *J. Phys. Chem. C* **2009**, *113*, 5805.

[47] P. Remón, R. Ferreira, J.-M. Montenegro, R. Suau, E. Pérez-Inestrosa, U. Pischel, *ChemPhysChem* **2009**, *10*, 2004.
[48] In a similar manner, a slower *o,o'*-diborylation reaction of 4-cyanobenzaldehyde *N,N*-dimethylhydrazone was observed; see: A. Ros, R. López-Rodríguez, B. Estepa, E. Álvarez, R. Fernández, J. M. Lassaletta, *J. Am. Chem. Soc.* **2012**, *134*, 4573.
[49] K. L. Billingsley, T. E. Barder, S. L. Buchwald, *Angew. Chem.* **2007**, *119*, 5455; *Angew. Chem. Int. Ed.* **2007**, *46*, 5359.
[50] L. Zhu, S. H. Shabbir, M. Gray, V. M. Lynch, S. Sorey, E. V. Anslyn, *J. Am. Chem. Soc.* **2006**, *128*, 1222.
[51] M. Montalti, A. Credi, L. Prodi, M. T. Gandolfi, *Handbook of Photochemistry*, 3rd ed., Taylor & Francis, Boca Raton, **2006**.
[52] A. A. Abdel-Shafi, F. Wilkinson, *Phys. Chem. Chem. Phys.* **2002**, *4*, 248.
[53] Z. R. Grabowski, K. Rotkiewicz, W. Rettig, *Chem. Rev.* **2003**, *103*, 3899.
[54] K. A. Zachariasse, *Chem. Phys. Lett.* **2000**, *320*, 8.
[55] P. Suppan, N. Ghoneim, *Solvatochromism*, The Royal Society of Chemistry, Cambridge, **1997**.
[56] C. Reichardt, *Solvents and Solvent Effects in Organic Chemistry*, 2nd ed., Wiley-VCH, Weinheim, **1990**.
[57] N. Mataga, Y. Kaifu, M. Koizumi, *Bull. Chem. Soc. Jpn.* **1956**, *29*, 465.
[58] E. Lippert, *Z. Naturforsch.* **1955**, *A10*, 541.
[59] Recently, it was shown that the addition of acetic acid to *ortho*-aminomethyl arylboronic acids can lead to simultaneous nitrogen protonation and carboxylate coordination at the boron center; see: B. E. Collins, S. Sorey, A. E. Hargrove, S. H. Shabbir, V. M. Lynch, E. V. Anslyn, *J. Org. Chem.* **2009**, *74*, 4055. However, with TFA, such a phenomenon was discarded based on the invariable ^{11}B NMR signal of compound **9** (as an example) in the absence and presence of TFA. On the other hand, ^{1}H NMR spectroscopy revealed clear evidence for the protonation of the isoquinoline moiety.
[60] A. Yuchi, A. Tatebe, S. Kani, T. D. James, *Bull. Chem. Soc. Jpn.* **2001**, *74*, 509.
[61] N. DiCesare, J. R. Lakowicz, *J. Phys. Chem. A* **2001**, *105*, 6834.
[62] C. Bresner, J. K. Day, N. D. Coombs, I. A. Fallis, S. Aldridge, S. J. Coles, M. B. Hursthouse, *Dalton Trans.* **2006**, 3660.
[63] S. Nave, R. P. Sonawane, T. G. Elford, V. K. Aggarwal, *J. Am. Chem. Soc.* **2010**, *132*, 17096.
[64] E. Galbraith, T. D. James, *Chem. Soc. Rev.* **2010**, *39*, 3831.
[65] J. V. Morris, M. A. Mahaney, J. R. Huber, *J. Phys. Chem.* **1976**, *80*, 969.
[66] Gaussian 03, Revision E.01, M. J. Frisch, G. W. Trucks, H. B. Schlegel, G. E. Scuseria, M. A. Robb, J. R. Cheeseman, J. A. Montgomery Jr., T. Vreven, K. N. Kudin, J. C. Burant, J. M. Millam, S. S. Iyengar, J. Tomasi, V. Barone, B. Mennucci, M. Cossi, G. Scalmani, N. Rega, G. A. Petersson, H. Nakatsuji, M. Hada, M. Ehara, K. Toyota, R. Fukuda, J. Hasegawa, M. Ishida, T. Nakajima, Y. Honda, O. Kitao, H. Nakai, M. Klene, X. Li, J. E. Knox, H. P. Hratchian, J. B. Cross, V. Bakken, C. Adamo, J. Jaramillo, R. Gomperts, R. E. Stratmann, O. Yazyev, A. J. Austin, R. Cammi, C. Pomelli, J. W. Ochterski, P. Y. Ayala, K. Morokuma, G. A. Voth, P. Salvador, J. J. Dannenberg, V. G. Zakrzewski, S. Dapprich, A. D. Daniels, M. C. Strain, O. Farkas, D. K. Malick, A. D. Rabuck, K. Raghavachari, J. B. Foresman, J. V. Ortiz, Q. Cui, A. G. Baboul, S. Clifford, J. Cioslowski, B. B. Stefanov, G. Liu, A. Liashenko, P. Piskorz, I. Komaromi, R. L. Martin, D. J. Fox, T. Keith, M. A. Al-Laham, C. Y. Peng, A. Nanayakkara, M. Challacombe, P. M. W. Gill, B. Johnson, W. Chen, M. W. Wong, C. Gonzalez, J. A. Pople, Gaussian, Inc., Wallingford, CT, **2004**.
[67] T. J. Bleisch, C. A. Clarke, J. A. Dodge, S. A. Jones, J. E. Lopez, C. W. I. Lugar, B. S. Muehl, T. I. Richardson, Y. K. Yee, K.-L. Yu (Eli Lilly and Company, Indianapolis), WO/2007/087488.
[68] J. A. Lowe III, W. Qian, S. E. Drozda, R. A. Volkmann, D. Nason, R. B. Nelson, C. Nolan, D. Liston, K. Ward, S. Faraci, K. Verdries, P. Seymour, M. Majchrzak, A. Villalobos, W. F. White, *J. Med. Chem.* **2004**, *47*, 1575.
[69] M. C. Carreño, J. L. García-Ruano, G. Sanz, M. A. Toledo, A. Urbano, *J. Org. Chem.* **1995**, *60*, 5328.
[70] Following the procedure described in ref. [69], a solution of *N,N*-dimethylnaphthalen-1-amine (342 mg, 2 mmol) in MeCN (10 mL) was treated with *N*-bromosuccinimide (392 mg, 2.2 mmol) and the reaction mixture was stirred 2 h at room temperature. Then, the reaction mixture was concentrated to dryness and purification by flash chromatography on silica gel (*n*-hexane/toluene, 1:1) gave 4-bromo-*N,N*-dimethylnaphthalen-1-amine (364 mg, 73% yield) as a yellow oil.
[71] J. Moursounidis, D. Wege, *Aust. J. Chem.* **1988**, *41*, 235.
[72] The stock solution of the catalyst was prepared by dissolving 2-pyridinecarboxaldehyde *N,N*-dibenzylhydrazone (37.6 mg, 0.125 mmol) and $[\{Ir(\mu\text{-}OMe)(cod)\}_2]$ (41 mg, 0.063 mmol) in dry THF to give a solution with a total volume of 25 mL (sonication for 1 h was used to accelerate the dissolution). The red-brown solution was kept under an argon atmosphere.

Received: October 30, 2012
Published online: March 28, 2013

